CHAPTER 3

Examination of the Effect of Arene Electronics on Aryl-Oxygen Bond Activation in Catalytic and Model Nickel(0) Diphosphine Systems

Abstract

Studies of the kinetics of oxidative addition using a series of nickel(0) (diphosphine)aryl methyl ether complexes with electron donating and withdrawing groups were undertaken. The observed rates and activation parameters for aryl-oxygen bond activation were found to be independent of the electronics of the ring the metal is coordinated to. The rate was found to depend on the electronics of the leaving alkoxide. The lack of variation with electronics in the model system is believed to be due to the simultaneous stabilization of the ground state and oxidative addition transition state. Relative rates for the cross coupling of anisoles with the $Ni(II)(PCy_3)_2Cl_2$ catalytic system were obtained for para-substituted anisoles for comparison to the stoichiometric system. Anisoles containing electron-withdrawing groups were found to be cleaved faster than those containing electron-donating groups in the catalytic system. The difference in rates was attributed to the differences in the strength of the nickel arene interactions. This was corroborated with equilibrium studies with substituted arenes.

INTRODUCTION:

Functionalization of the aryl carbon oxygen bonds has emerged as a versatile synthetic tool in organic methodology as phenol precursors are readily available and synthetic modification of the aromatic ring is facile.[1] Aryl carbon oxygen bonds, however, are strong and difficult to activate. Nickel based catalysts have been shown to be versatile in the cleavage of aryl carbon oxygen bonds in a variety of different moieties.[1-8] The cleavage of the aryl carbon oxygen bond can be followed by the coupling of the substrate with a variety of cross-coupling partners.[1,3-7,9] While the mechanism of palladium cross-coupling have been studied extensively, fewer mechanistic studies have been carried out on nickel catalyzed cross coupling systems.[10-13] It is imperative to carry out such studies as nickel and palladium, while both group 10 metals have different reactivity profiles. For example, the smaller more nucleophilic nickel center more readily harnesses phenol-derived and less reactive electrophiles in cross coupling. Furthermore, nickel centers undergo such reactions using less exotic ligands than the palladium counterparts, in some cases ligand free conditions can be used.[1] These factors, combined with its low cost, make nickel an ideal metal for cross coupling and activation of aryl reagents.[1] Detailed mechanistic studies of nickel catalyzed aryl carbon oxygen bond activation will result in the design of better catalysts for said activation, which, as fore mentioned, is important for organic methodology and for other applications such as biomass conversion as Hartwig demonstrated.[14]

Previously we reported a nickel(0) meta-terphenyl diphosphine complex containing an aryl ether functionality on the ipso carbon of the central aryl ring. Using this system it was shown that with heating the Ni center was able to undergo a subsequent oxidative addition, followed by a beta-hydrogen elimination, and an assisted reductive elimination

and decarbonylation.[15] As this system undergoes several steps important to nickel aryl carbon oxygen bond activation relevant to cross-coupling and biomass conversion, studies of the oxidative addition were undertaken using this nickel model system.[1] Herein is described the stoichiometric oxidative addition studies as well as the efforts to compare the model studies with data obtained from nickel catalysts.

RESULTS & DISCUSSION:

Our previously described series of nickel(0) model system, which undergoes a stoichiometric intramolecular reductive cleavage of an aryl oxygen bond, provides an ideal scaffold to study nickel facilitated oxidative addition. Variation of the electronics of the terphenyl backbone can make the observed oxidative addition similar to the activation of substrates with varying aryl electronics. To this end several nickel(0) complexes were synthesized containing different functional groups on the central arene, para to the ipso methyl ether. The functional groups were selected to cover the range of the Hammett parameters with the dimethyl amino group being the most electron donating group (EDG) and trifluoromethyl being the most electron withdrawing group (EWG) (Table 1).

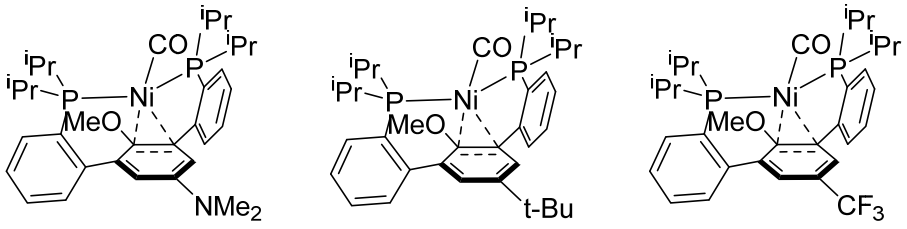

R =	NMe_2	t-Bu	CF_3
σ_p	-0.83	-0.20	0.54
ν_{CO} (cm^{-1})	1912	1919	1943

Table 3.1 Hammett parameters and carbonyl stretching frequencies of **16**, **16**$_{tBu}$, and **16**$_{CF3}$

The EDG and EWG on the central arene should modulate the strength of the metal arene interaction as a more electron deficient ring should have a stronger metal arene interaction. In order to probe the effect of the electronics on the central arene ring the carbonyl complexes **16**, **16**$_{tBu}$, and **16**$_{CF3}$ were synthesized. The carbonyl

stretching frequency will give a measure of the strength of the nickel arene interaction. The carbonyl complexes were synthesized through the decarbonylation of paraformaldehyde by the nickel(0) terphenyl diphosphines **2**, $\mathbf{2}_{t\mathrm{Bu}}$, and $\mathbf{2}_{\mathrm{CF3}}$ in THF. The rates of decarbonylation in **2**, $\mathbf{2}_{t\mathrm{Bu}}$, and $\mathbf{2}_{\mathrm{CF3}}$ varied with the electronics, with NMe_2 being much faster than CF_3. Measuring the carbonyl stretching frequencies of the three nickel variants by IR spectroscopy gave the stretching frequencies listed in table 3.1.

A low carbonyl stretching frequency is indicative of backbonding between the metal and carbonyl. Backbonding occurs between the metal and the π^*-orbital of the C-O bond. Donation into this orbital leads to a weakening of the C-O bond and a strengthening of the M-C bond. Similarly the metal binds to the central arene through donation of electron density into the π^*-orbital of the central arene ring which leads to an elongation of the central arene bond the metal interacts with. As σ_p of the arene increases ν_{CO} increases, which is consistent with less backbonding between the metal and the carbonyl and more backbonding to the arene. The backbonding gives an estimate of the metal arene interation as a stronger interaction leads to a higher ν_{CO} closer to the stretch of free CO (ν_{CO} = 2143 cm^{-1}). The stretching frequencies for the NMe_2 and t-Bu variants are quite low, indicative of a weaker nickel arene interaction. The ν_{CO} stretching frequencies are also very similar (1912 vs. 1919 cm^{-1}) although the Hammett parameters of the two are vastly different ($\sigma_{p\Delta}$ = -0.63). Substitution of a trifluoromethyl group in the central ring as in $\mathbf{16}_{\mathrm{CF3}}$ leads to a stronger nickel arene interaction and conversely a stronger ν_{CO} (1943 cm^{-1}).

The kinetics of oxidative addition in these model systems was investigated. The kinetics are believed to be first order as the observed reaction is **2** going to **3** (Scheme

3.1). **2** was dissolved in d_6-benzene and heated to 45 °C in a J-Young tube. The decay of **2** to **3** was monitored by ^{1}H NMR spectroscopy. Under the described conditions the oxidative addition of the nickel undergoes three half-lives in ca. 14 hours. At 45°C the observed rate of oxidative addition in **2** was found to be 2.09 ± 0.05 min^{-1}, while the k_{obs} for $\mathbf{2_{tBu}}$ was 2.38 ± 0.05 min^{-1}. While the oxidative addition in **2** and $\mathbf{2_{tBu}}$ was facile at 45 °C, oxidative addition was too slow in $\mathbf{2_{CF3}}$. The kinetic studies for the oxidative addition in the **2** and $\mathbf{2_{tBu}}$ suggest that there is little difference between the measured rates.

Scheme 3.1 Oxidative addition in the nickel(0) model system 2

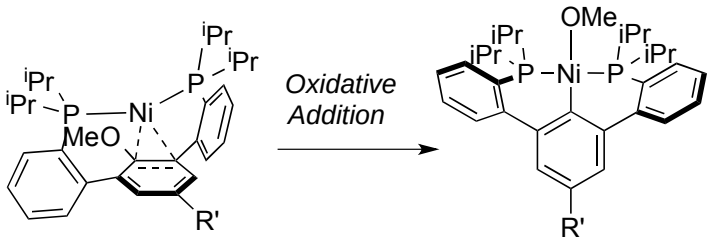

2 R'= NMe_2 **3** R'= NMe_2
$\mathbf{2_{tBu}}$ R'= tBu $\mathbf{3_{tBu}}$ R'= tBu
$\mathbf{2_{CF3}}$ R'= CF_3 $\mathbf{3_{CF3}}$ R'= CF_3

Attempts were also made to study the rate of oxidative addition at higher temperatures. At 80°C the k_{obs} of oxidative addition in **2** was found to be 83 ± 2 min^{-1} while the rates for $\mathbf{2_{tBu}}$ and $\mathbf{2_{CF3}}$ were found to be 72.3 ± 0.4 min^{-1} and 18.3 ± 0.2 min^{-1} respectively. The oxidative addition at 80°C is about 30 times faster than the determined rates at 45°C and the oxidative addition is complete after ca. 40 minutes. After collecting data on the oxidative addition at 45°C and 80°C, an attempt was made to perform a similar ^{1}H NMR kinetic analysis at 60°C. At 60°C, however, during the course of the oxidative addition significant impurities were detected. Analysis of the ^{31}P NMR spectrum collected after the depletion of **2** shows several phosphorus peaks of

unknown identity. In the ^{31}P NMR spectrum peaks, are observed at 38.59, 36.26, 34.15, 30.92, and finally 27.24 ppm (Figure 1). The peaks at 34.15 and 27.24 ppm correspond to **6** and the **3** respectively. The peak at 38.59 ppm corresponds to complex **7** while the peak at 30.92 ppm is assigned to a nickel(II) chloride, which is a decomposition product of the hydride in dichloromethane. The identity of the species that produces the peak at 36.26 ppm in the ^{31}P NMR spectrum was found to be the nickel(0)-carbonyl complex **16** by independent synthesis (Scheme 3.2).

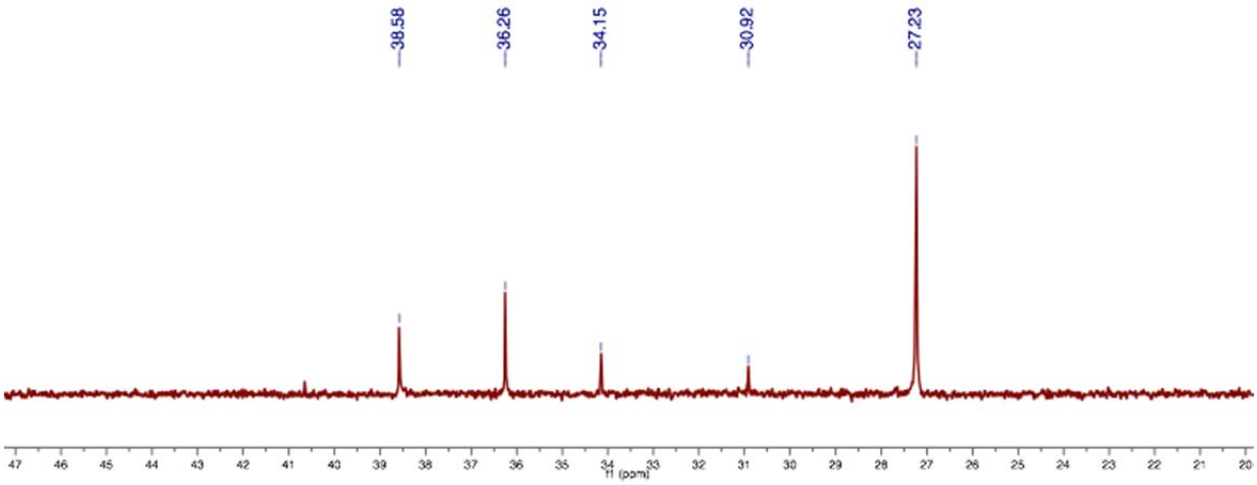

Figure 3.1: ^{31}P{^{1}H} NMR spectrum of the products of **2** at 60°C. 27.23 ppm is **3**. 30.92 ppm possible nickel(II) chloride impurity, 34.15 ppm **6**, 36.26 ppm **16**, and 38.58 ppm is the reductive elimination product of the Ni(II) hydride **7**.

Scheme 3.2 Synthesis of 16 from 2 and formaldehyde

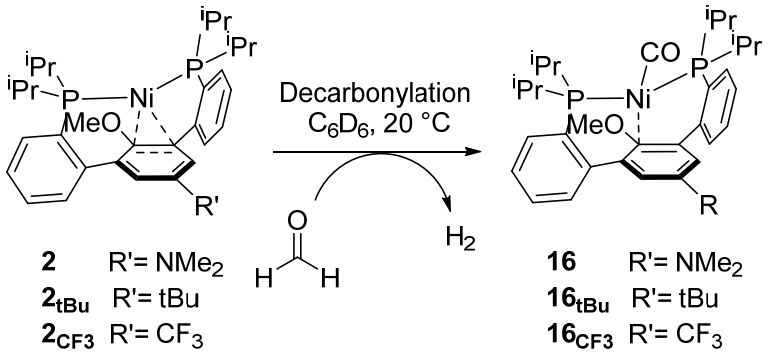

Previously the only reactivity of the nickel(0) diphosphine terphenyl species observed was the described intramolecular oxidative addition. However, **2,** at room temperature, can react with formaldehyde to undergo decarbonylation to form complex **16** (Scheme 3.2). Examination of the ^{1}H NMR for **16** gives a spectrum similar to **6** albeit with an indicative peak at 2.57 ppm, which is identified as the methoxy peak by integration. Both nickel(0)-carbonyl complexes show central aryl ring resonances at similar chemical shifts (6.58 ppm for **16** vs. 6.52 ppm for **6**). IR spectroscopy analysis of the **16** reveals a stretching frequency of 1912 cm^{-1}, which was confirmed by independent synthesis (Table 3.1). This stretching frequency is in the range of **6** and **6$_{tBu}$** (1917 cm^{-1} and 1929 cm^{-1} respectively) albeit lower as an increase in backbonding from the Ni center to the CO is consistent with a more electron rich central arene *vide supra*. **16** is quite stable at the temperatures of the kinetic experiments (no change by ^{31}P and ^{1}H NMR spectroscopy after 9 days at 80°C). Decarbonylation of formaldehyde by **2** is concerning, as the reaction of **2** will increase the observed rate for the oxidative addition, as **2** is participating in two different reactions.

Interestingly, the reaction of the Ni^{0} at 45°C or 80°C produces little of the **16** impurity. Close analysis of the ^{31}P NMR spectra of the reaction at 45°C reveals the

formation of a small amount of the nickel(II) hydride **4** and **16** and minuscule amounts of **7**. Only **16** affects the rate of oxidative addition as it is the only impurity derived from the **2**. The concentration of **16** in solution is miniscule in comparison to the remaining **1** starting material and the oxidative addition product **3**. Similarly at 80°C few impurities are generated and the end product is **6**. It is interesting how the interplay of the relative rates of oxidative addition and the beta-hydrogen elimination allow for the relatively clean reactions at 45°C and 80°C and a messy reaction at 60°C. At 45°C the rate of beta-hydrogen elimination is apparently slow compared to oxidative addition thus hindering the formation of **16**. Increasing the temperature to 80°C drastically increases the rate of oxidative addition which becomes much faster than beta-hydrogen elimination and when formaldehyde is formed from the beta-hydrogen elimination there is no **2** remaining to react with. At 60°C however, beta-hydrogen elimination proceeds at an observable pace and oxidative addition is not fast enough resulting in the generation of significant amounts of formaldehyde which proceeds to undergo decarbonylation with **2** to form the observed complex **16** (Scheme 3.3).

Scheme 3.3 Reactivity of 2 at 60 °C

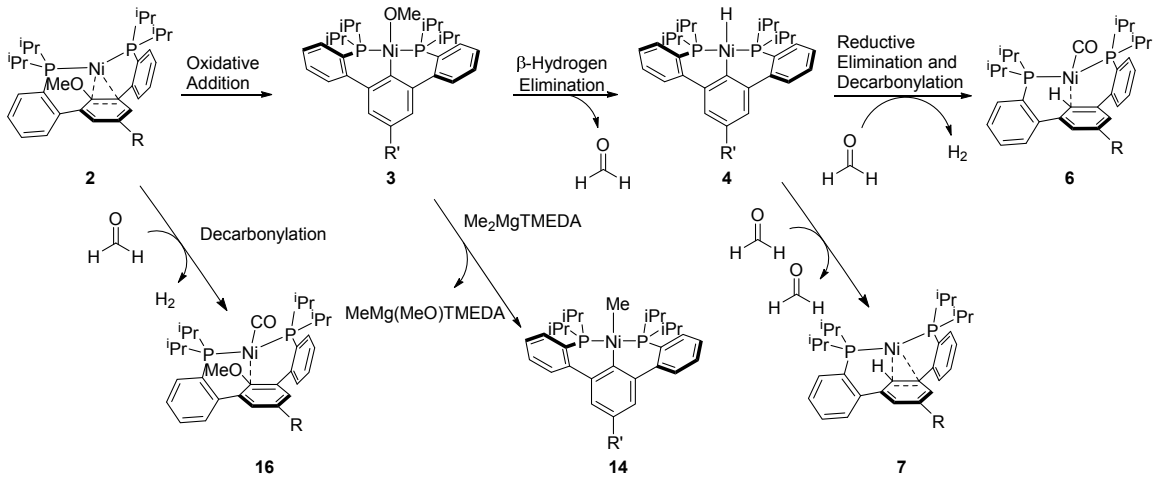

The formation of **16** from formaldehyde significantly hinders the kinetic analysis of the intramolecular oxidative addition of **2**. In order to inhibit the formation of **16**, complex **3** was reacted with a transmetallation reagent to prevent formaldehyde formation (Scheme 3.3). The addition of Me_2MgTMEDA to a solution of **2** produced no reaction at room temperature as determined by ^{31}P and ^{1}H NMR spectroscopy. Heating this mixture to 45°C led to the exclusive formation of a new species at 44.46 ppm by ^{31}P NMR spectroscopy. This species was identified as a nickel(II) methyl complex (**14**) by the upfield triplet at -0.38 ppm in the ^{1}H NMR spectrum. The observed triplet is consistent with a nickel methyl with splitting from the coordinated phosphine groups. It was hypothesized that transmetallation would be fast with respect to oxidative addition and beta-hydride elimination, indeed the reaction of **2** with Me_2MgTMEDA at 80°C for one hour leads to the formation of **14** as the sole product.

Further heating of **14** at 80°C leads to the formation of a new species as identified by ^{31}P and ^{1}H NMR spectroscopy (Scheme 3.4). Heating the Ni-Me complex several hours at 80°C leads to the observation of a new resonance at 36.85 ppm in the ^{31}P NMR spectrum. If the heating is continued for ca. 48 hours complex **14** can be

completely converted to this new species **10**, which was characterized as the product of a reductive elimination of **14** by ^{1}H NMR spectroscopy and ESI-MS. Analysis of the ^{1}H NMR spectrum of **10** shows two indicative peaks, a peak at 1.47 ppm, consistent with the aryl methyl, and a peak for the central arene at 5.76 ppm, which is consistent with the nickel center interacting with the central arene (the central arene of **2** gives a peak at 5.85 ppm by ^{1}H NMR spectroscopy).

Scheme 3.4 Reductive elimination of 14 to form nickel(0) complex 8

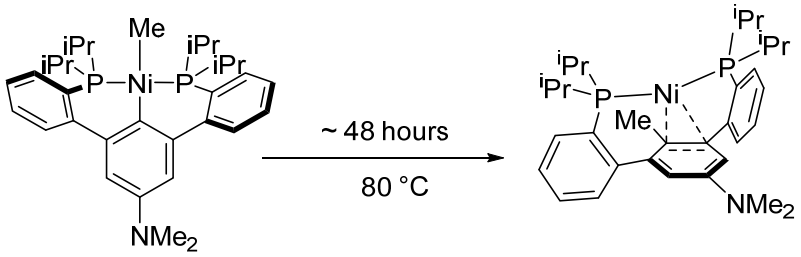

14 **10**

Using Me_2MgTMEDA as a transmetallation agent another attempt was made to measure the kinetics of intramolecular oxidative addition of **2** at 60°C. When 1.2 eq. of Me_2MgTMEDA was used a rate of $k = 10.5\text{x}10^{-3}$ min^{-1} was obtained from observing the decay of **2** by ^{1}H NMR spectroscopy (Table 3.2). To examine the possibility that the Me_2MgTMEDA is somehow affecting the rate of the oxidative addition, the rate was measured using different concentrations of the transmetallation agent. Using 10 and 23 eq. of Me_2MgTMEDA rate constants of $k = 10.2\text{x}10^{-3}$ min^{-1} and $k = 10.7\text{x}10^{-3}$ min^{-1} were obtained respectively. If the Me_2MgTMEDA was affecting the rate constant one would expect to observe a significant change in the rate with increasing concentration of transmetallating agent. From the rate constant data it appears that the addition of Me_2MgTMEDA does not affect the rate constant of oxidative addition in **2** at a given temperature.

Complex	Equivalents of $Me_2MgTMEDA$	Temp °C	k_{obs} (min^{-1})
2	1	60	$10.5x10^{-3}$
2	10	60	$10.2x10^{-3}$
2	23	60	$10.7x10^{-3}$

Table 3.2: Observed rate constants for the oxidative addition of **2** in the presence of varying amounts of $Me_2MgTMEDA$ in C_6D_6 at 60°C.

Rates of Oxidative addition from the Ni^0 model system

As MeMgTMEDA was shown to have no effect on oxidative addition rates of oxidative addition were measured at 45, 70, and 80°C (Figure 3.2) of which the results are shown in table 3.3. The rates at 45 and 80 °C without MeMgTMEDA were found to compare well with rates observed with MeMgTMEDA (2.09 ± 0.05 and 83 ± 2 vs. 2.19 ± 0.05 and 86 ± 3 (x 10^{-3})(min^{-1}) respectively). From these rates the activation parameters $\Delta H^{\ddagger}$ and $\Delta S^{\ddagger}$ were calculated using the linear form of the Eyring correlation (Equation 3.1 B, Figure 3.3, and Table 3.4).

Equation 3.1

A) $$k = \frac{k_B T}{h} \exp\left(\frac{\Delta S^{\ddagger}}{R}\right) \exp\left(-\frac{\Delta H^{\ddagger}}{RT}\right)$$

B) $$\ln\frac{k}{T} = \frac{-\Delta H^{\ddagger}}{R} \cdot \frac{1}{T} + \ln\frac{k_B}{h} + \frac{\Delta S^{\ddagger}}{R}$$

Analogous studies were undertaken using the previously synthesized tert-butyl variant $\mathbf{2}_{t\mathrm{Bu}}$. The rates of oxidative addition were measured in the presence of dimethyl magnesium TMEDA at 45, 60, and 80°C the observed rates and calculated activation parameters $\mathbf{2}_{t\mathrm{Bu}}$ are listed in tables 3.3 and 3.4 respectively. In the case of the para-

trifluoromethyl substituted $\mathbf{2}_{CF3}$ it was observed that the addition of Grignard resulted in the loss of ^{1}H and ^{31}P NMR resonances possibly due to the formation of a paramagnetic species. Due to this reactivity the rates of oxidative addition were obtained without the addition of a transmetallating agent. Fortunately, $\mathbf{2}_{CF3}$ reacts much slower with formaldehyde than either **2** or $\mathbf{2}_{tBu}$. The rates of oxidative addition obtained from $\mathbf{2}_{CF3}$ were found to be only three times slower than that for **2** or $\mathbf{2}_{tBu}$ (Table 3.3).

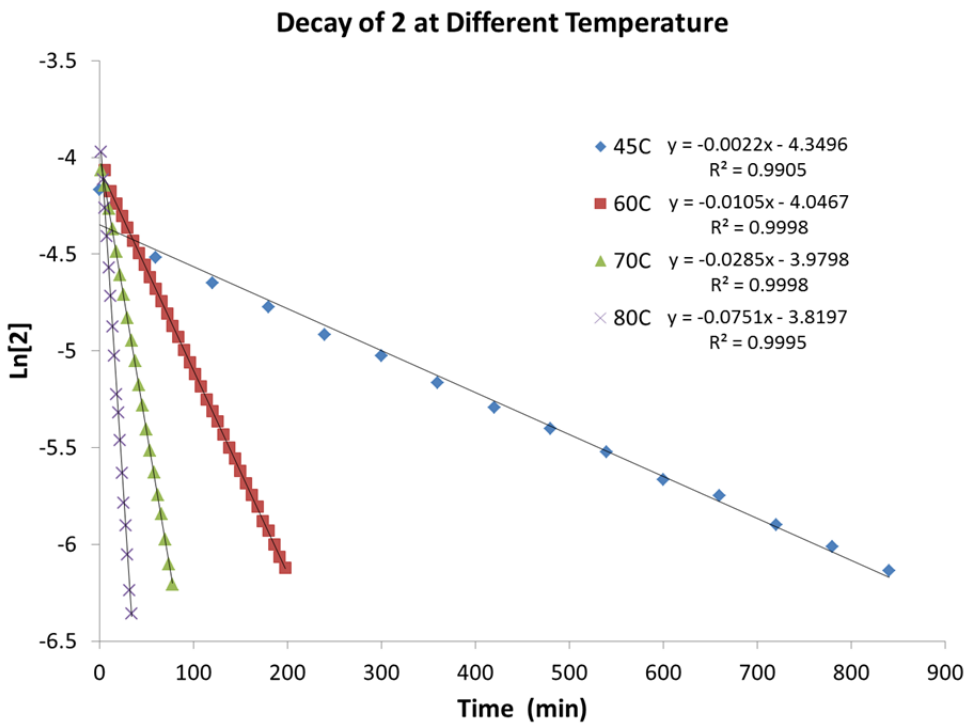

Figure 3.2: Kinetic plots of the first order Decay of **2** at 318, 333, 343, and 353 K.

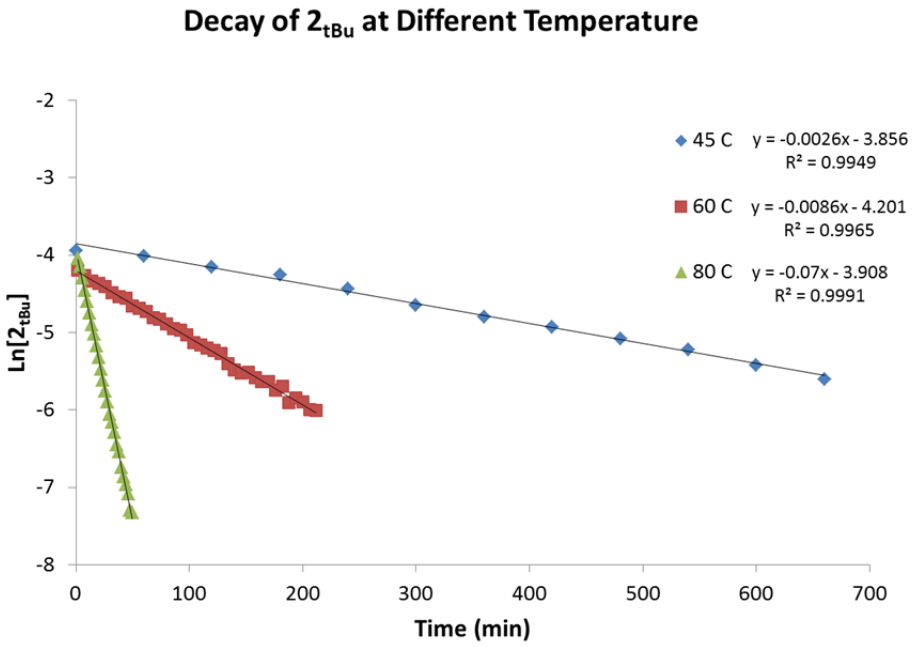

Figure 3.3: Kinetic plots of the first order Decay of $\mathbf{2}_{tBu}$ at 318, 333, and 353 K.

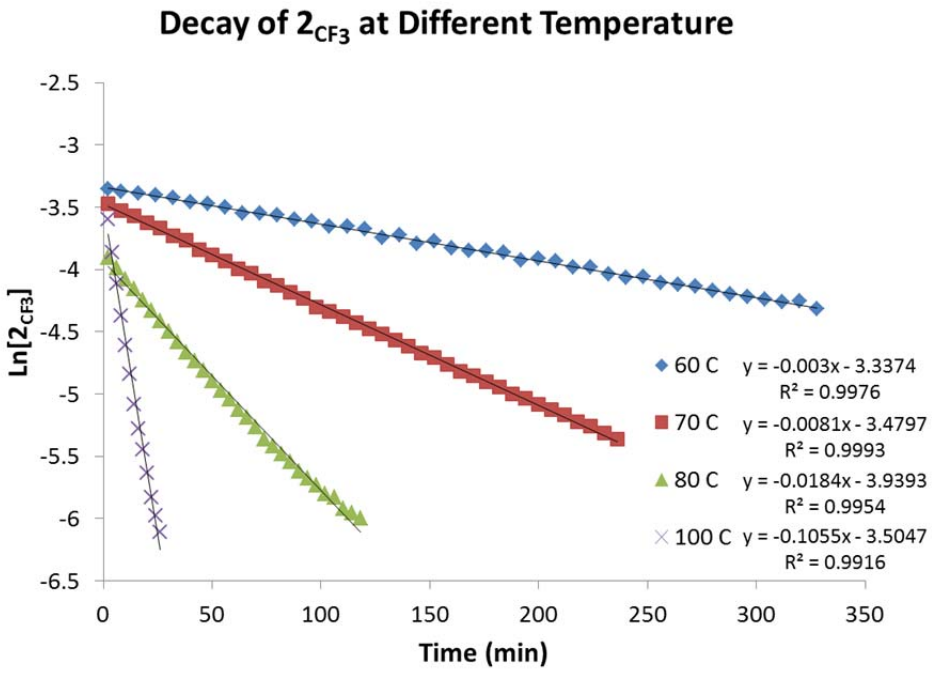

Figure 3.4: Kinetic plots of the first order Decay of 2_{CF3} at 333, 343, 353, and 373 K.

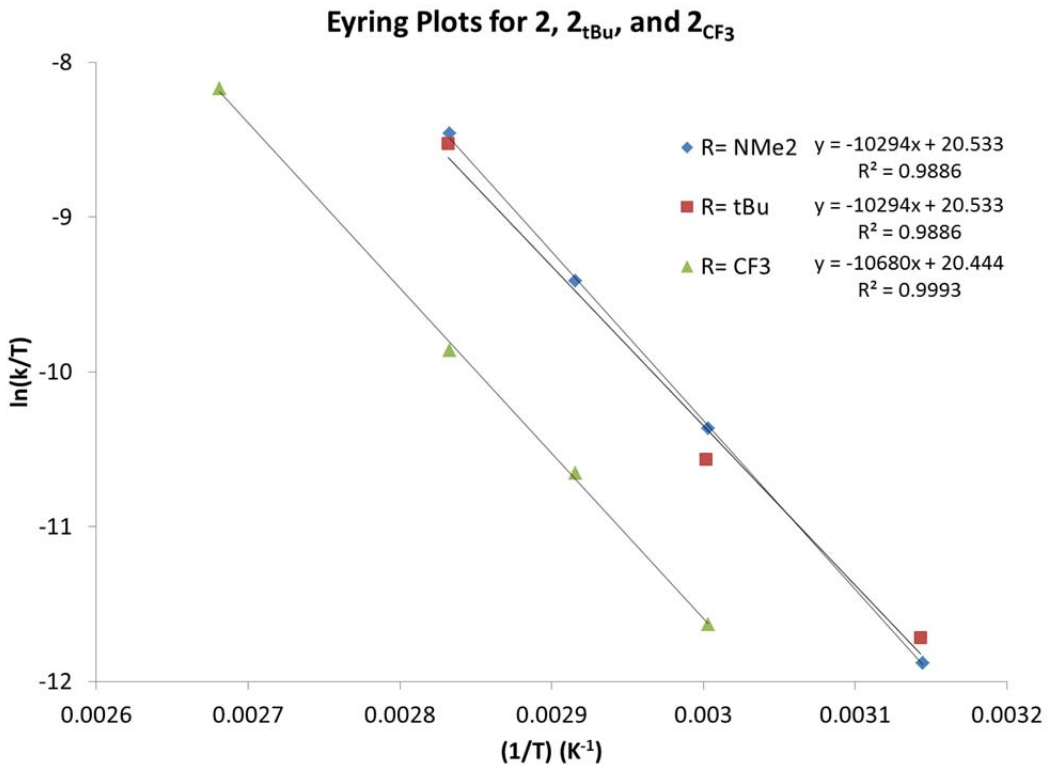

Figure 3.5: Eyring plots of **2**, 2_{tBu}, and 2_{CF3}

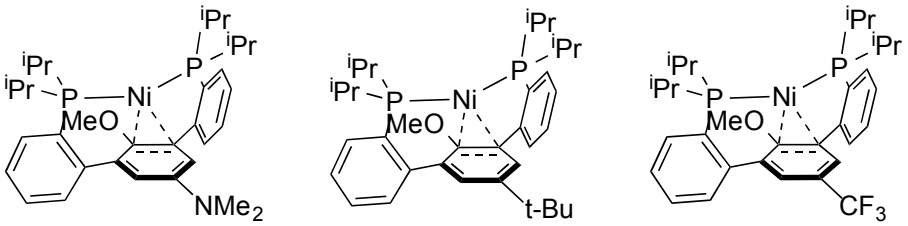

R=	NMe_2	t-Bu	CF_3
T= (K)	k_{obs} (min^{-1}) ($x10^{-3}$)	k_{obs} (min^{-1}) ($x10^{-3}$)	k_{obs} (min^{-1}) ($x10^{-3}$)
318	2.19 ± 0.05	2.58 ± 0.05	-
333	10.2 ± 0.1	8.65 ± 0.09	2.94 ± 0.04
343	28.4 ± 0.1	-	8.05 ± 0.05
353	86 ± 3	70.0 ± 0. 4	18.3 ± 0.2
363	-	-	-
373	-	-	105 ± 3

Table 3.3 Observed rate constants for **2**, $\mathbf{2}_{tBu}$, and $\mathbf{2}_{CF3}$ at different temperatures

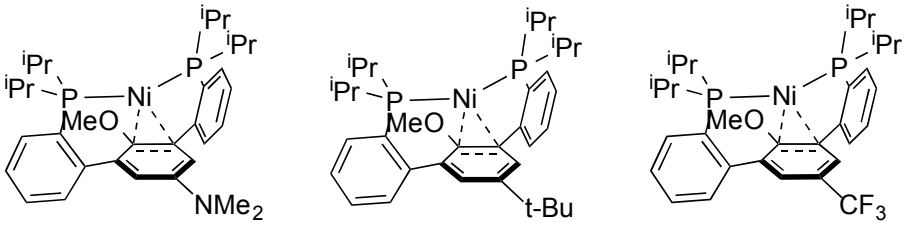

	NMe_2	t-Bu	CF_3
$\Delta H^{\ddagger}$(kcal mol^{-1})	21.7 ± 0.2	20 ± 2	21.2 ± 0.4
$\Delta S^{\ddagger}$(cal K^{-1} mol^{-1})	-2.66 ± 0.03	-6 ± 1	-6.6 ± 0.2

Table 3.4 Calculated activation parameters for **2**, $\mathbf{2}_{tBu}$, and $\mathbf{2}_{CF3}$

As can be seen from table 3.3 the rates of oxidative addition in the model systems are quite similar between the dimethylamino, tert-butyl, and trifluoromethyl groups with the trifluoromethyl group being only three times slower, despite the electronics being significantly different. Consequently the obtained activation parameters are all within error of each other. The similarities of the activation parameters could arise due to a stabilization of the nickel(0) ground state as shown in figure 3.4. This ground state stabilization arises due to the nickel arene interactions.

The nickel arene interactions could also lead to stabilization of the transition state of the aryl oxygen bond activation. But if both the ground state and transition state were stabilized similarly, overall it would appear as if there was little to no effect of electronics, which is the case in the model system. For example, **1** would form a nickel(0) complex (**2**) that is less stable than the trifluoromethyl complex (**2**$_{CF3}$) due to weaker interactions with the central arene ring. From this complex the oxidative addition transition state may be destabilized by a similar energy. This trend of thought could also be applied to **2**$_{CF3}$, stabilization of the Ni^0 and stabilization of the intermediate by similar energies and the activation parameters observed in these complexes would end up being similar (Figure 3.2).

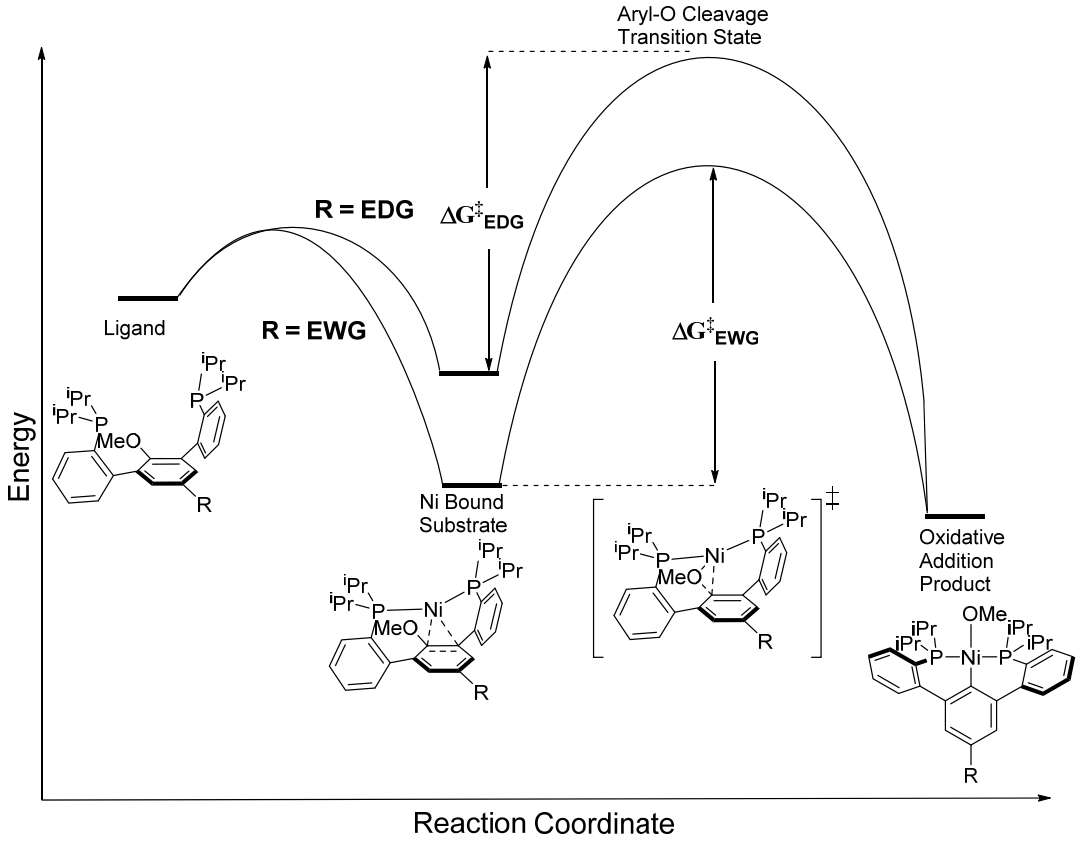

Figure 3.6 Hypothetical reaction coordinate diagram for oxidative addition in the studied nickel(0) model systems.

Given that the observed rate of oxidative addition was found to not be effected by the electronics of the arene that the nickel is coordinated to, an effort was made to change the electronics of the ether on the other side of the oxygen bond. To this end the kinetics of oxidative addition in the nickel(0) terphenyl diphosphine aryl ether complex **15** were investigated. **15** undergoes oxidative addition at 20 °C over the course of several hours to form **13**, and hence cannot be isolated *vide supra*. In order to obtain rates for oxidative addition in **15** a nickel(I) system based on the terphenyl diphosphine aryl ether backbone was used $\mathbf{9^{OAr}}$ (see Chapter 2). The nickel (I) system $\mathbf{9^{OAr}}$ can be synthesiszed via a comproportionation of $Ni(COD)_2$ and $NiCl_2(DME)$ with the diphosphine $\mathbf{1^{OAr}}$. Transmetallation of $\mathbf{9^{OAr}}$ with a Grignard leads to the formation of the reduced nickel complex **15** (presumably analoguous to the reduction observed in the forementioned nickel (I) complexes (see Chapter 2)). This method of generation of **15** was used to study the kinetics of oxidative addition.

Scheme 3.5 Synthesis of $\mathbf{9^{Oar}}$ from diphosphine $\mathbf{1^{OAr}}$

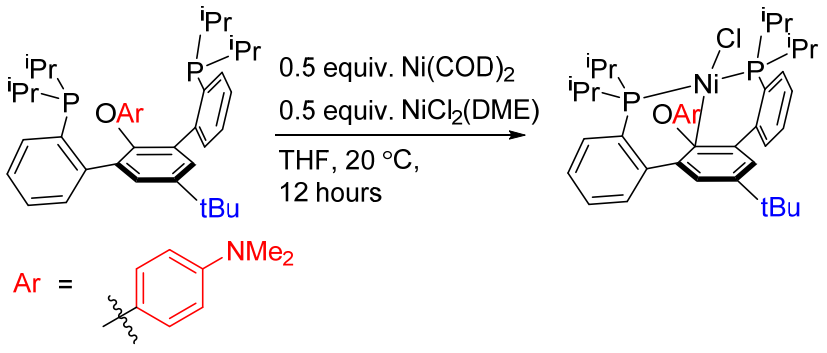

Oxidative addition was measured at 35, 40, 45, and 50°C of which the results are shown in table 3.5. The observed rates of oxidative addition in the aryl aryl ether were found to be about two orders of magnitude faster than the alkyl ethers (Table 3.5). Using the Eyring correlation (Equation 3.1) the activation parameters of the

oxidative addition were calculated as shown in table 3.6. The $\Delta H^{\ddagger}$ was found to be 19.8 ± 0.4 (k_{cal}/mol^{-1}) while $\Delta S^{\ddagger}$ was found to be 0.42 ± 1 (e.u.). The rate increase is believed to be in part due to the electronics of the phenoxide being a better leaving group than an alkoxide leading to faster oxidative addition. While the electronics of the nickel-coordinated arene have little effect on the observed rates the electronics of the ether greatly affect the favorability of oxidative addition.

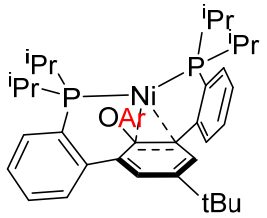

15

Temperature	k_{obs} (min^{-1})
35	0.066
40	0.108
45	0.186
50	0.310

$\Delta H^{\ddagger}$ (k_{cal}/mol^{-1})	19.8 ± 0.4
$\Delta S^{\ddagger}$ (e.u.)	0.4 ± 0.2

Table 3.5 (Left) Observed kinetics of oxidative addition in **15** at different temperatures (Right) Derived activation parameters for **15**

It is known from relative rates of palladium(0) and nickel(0) catalysts that the presence of an electron withdrawing group leads to an increase in the rate of catalysis.[16-19] One way of explaining this phenomenon in light of the data we observe, is that the starting points differ in each case. For our Ni^0 system we start with the metal center already coordinated to the substrate ligand, while in the case of the catalyst the Ni^0 is unbound. In the catalytic systems there is a fast pre-equilibrium which forms the nickel(0) arene adduct. This equilibrium is dependent on the electronics of the aryl substrate. The more electron deficient arenes form a stronger interaction with the

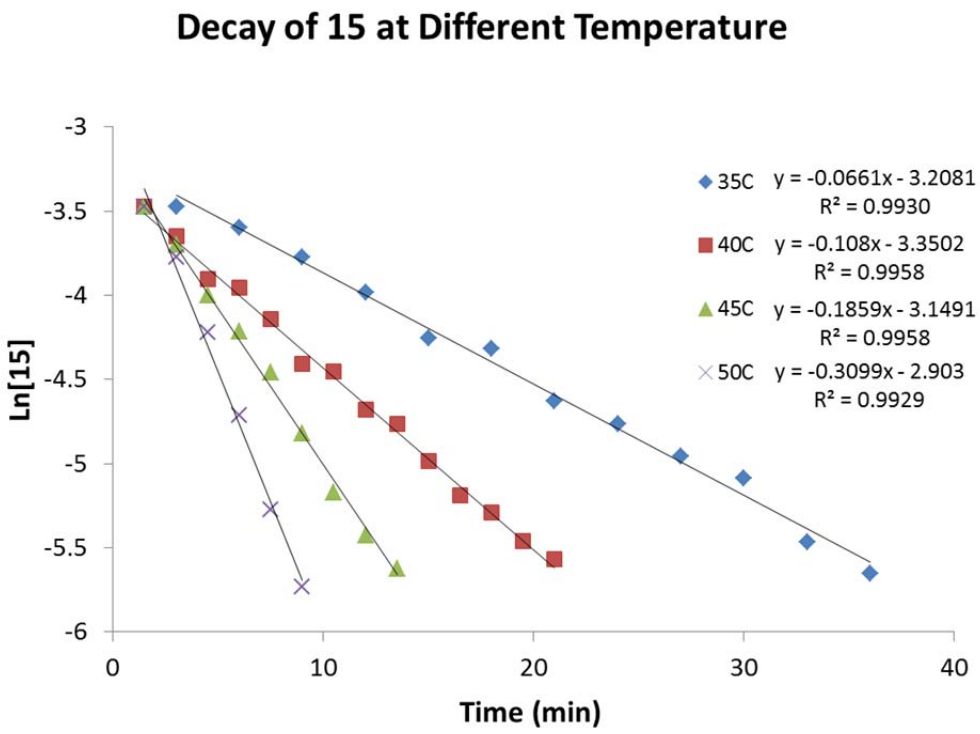

Figure 3.7: Kinetic plots of the first order Decay of **15** at 308, 313, 318, and 323 K.

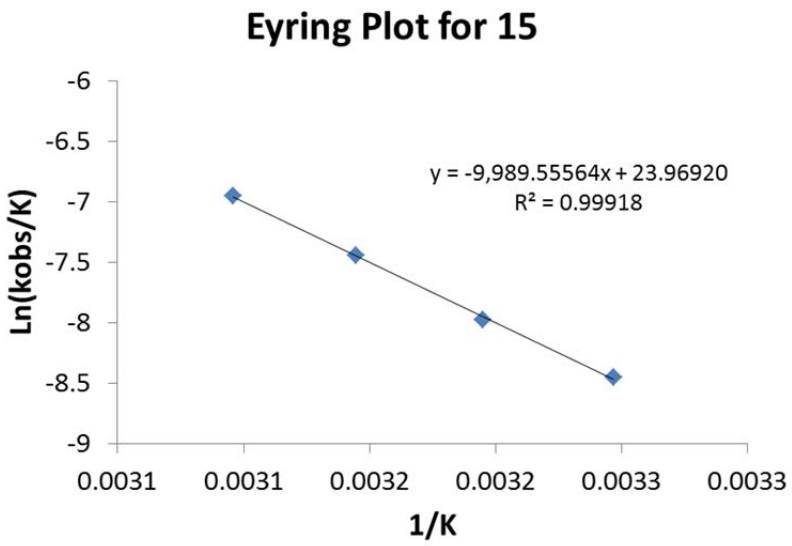

Figure 3.8: Eyring plot of **15**

nickel(0) center as shown with the nickel model systems *vide supra* (Table 3.1). This pre-equilibrium shifts the concentration of the nickel(0) arene species leading to an observed rate increase. In order to better understand the effect of the arene interactions in oxidative addition, studies were shifted from model systems to catalytic systems.

Nickel Catalyst Studies

Studies of oxidative addition in nickel catalyst systems were undertaken using two different nickel systems, the known and versatile cross coupling catalyst $Ni(II)(PCy_3)_2Cl_2$ **(17)**[1-7,9], and the structurally characterized $[Ni(PCy_3)_2]_2N_2$ complex **(18)**.[20] **17** is a known precatalyst for the Kumada coupling of aryl ethers and Grignard reagents (Scheme 3.6). It is proposed that **17** undergoes a sequential transmetallation to form a nickel(0) dialkyl species which undergoes reductive elimination leading to the formation of a nickel(0) species, which is believed to be the active catalyst. As **17** is a known catalyst for oxidative addition of anisoles, conditions similar to those found in literature were used. Initial catalysis screens yielded little to no conversion of the starting anisole. It was initially believed this limited activity could be due to the use of chloride containing Grignard reagents, however it was found that the presence of THF greatly hinders the activity of the catalyst. Removal of the THF from the Grignard reagent or the use of a Grignard containing diethyl ether resulted in catalytic activity. It was found from these initial studies that the trifluoromethyl anisole reacts faster than the dimethyl and tert-butyl variants. Similarly in 1:1 competition reactions conversion was only observed in the trifluoromethyl anisole, which indicates that the nickel

preferentially undergoes oxidative addition with the more electronegative substrate. Through competition reactions relative rates were obtained for a variety of substrates as shown in table 3.6.

Scheme 3.6 Proposed catalytic cycle for the Nickel catalyzed cross coupling of Aryl ethers with Alkyl Grignards

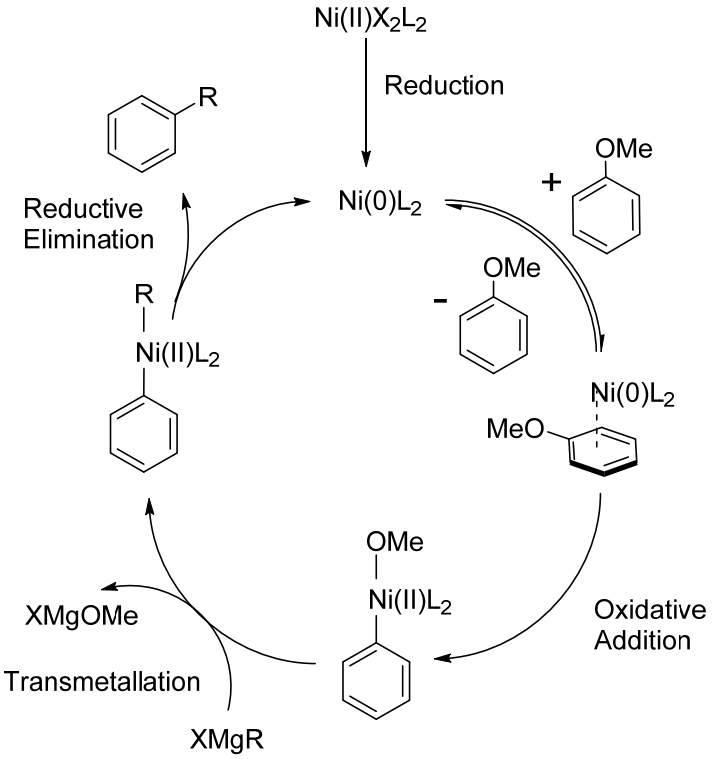

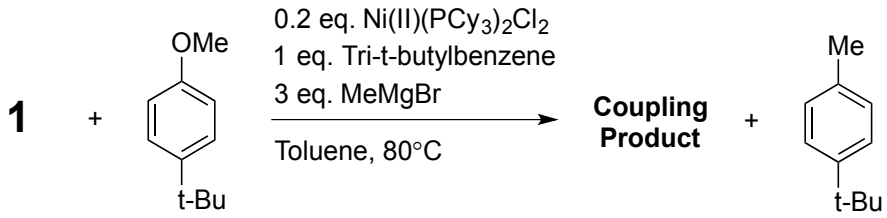

	Relative Rate$_{obs}$
Arene Electronics 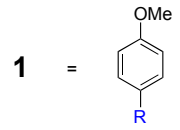	
NMe_2	1.07
CF_3	10.26
Arene Substitution 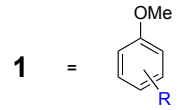	
4-Methyl	1.17
3-Methyl	1.23
2-Methyl	0.91
2,6-Methyl	0.34
Aryl Ether variation 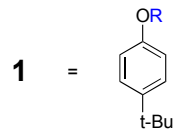	
Ethyl ether	0.90
Isopropyl ether	0.96
Trimethylsilyl ether	5.78
Carbamate	39.28
Arene Variation 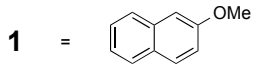	
2-Methoxynapthalene	65.00

Table 3.6 Relative rates obtained from competition reactions. All rates are relative to 4-tertbutyl anisole.

While oxidative addition is well documented for **17** it is not as well documented in the literature for oxidative addition to anisoles. For the catalysis from the $[Ni(PCy_3)_2]_2N_2$ complex **18**, conditions identical to those used for the $Ni(II)(PCy_3)_2Cl_2$ system were used. Gratifyingly, **18** was found to facilitate the coupling between an anisole and an alkyl Grignard in a fashion similar to **17**. In order to further probe oxidative addition in this system, attempts were made to directly observe oxidative addition via ^1H NMR spectroscopy in a similar fashion to the Ni model complexes i.e. a shifting of the arene or methoxy resonances. Unfortunately, no change was observed by ^1H NMR spectroscopy in a 1:1 mixture of tert-butyl anisole with **18** even when heating to 80 °C. Similarly no oxidative addition was observed to take place with trifluoromethyl anisole under similar conditions. While no oxidative addition was observed, the addition of methyl Grignard to a solution containing a catalytic amount of **18** resulted in a conversion of the tert-butyl anisole to the tert-butyl toluene. Surprisingly, one equivalent of the methyl Grignard did not result in a clean conversion of the anisole into toluene. Something similar was observed with aryl Grignards, as homo-coupled arenes were observed after the coupling reaction, when aryl Grignards were used. Although no ethane, the expected by product from methyl Grignard, was observed it is still possible homo-coupling or some other process is taking place.

The relative rates observed with the nickel systems **17** and **18** give a trend of increasing rate of reactivity with electron withdrawing substrates. This is in contrast with what was observed in our nickel model system. The observed rate of increase could be due to the nickel catalytic species having a better metal arene interaction with

the more electron withdrawing substrates as was inferred from the model complex. In order to understand the effects of the substrate pre-equilibrium (Scheme 3.6) the equilibrium constants of different arenes were investigated. One of the problems with the nickel precatalysts **17** and **18**, is the identity of the actual catalyst is unknown. The actual catalyst could be a nickel diphosphine or a nickel monophosphine, which would complicate the observed kinetics and equilibra, as phosphine dissociation/association with the catalytic species would become relevant. As phosphine dissociation/association could be a complicating factor a nickel(0) system containing a chelating diphosphine was used. Nickel(II)$(Cl)_2$(dcpe) (dcpe= 1,2-bis(dicyclohexylphosphino)ethane) can be treated with sodium naphthalene to form nickel(0)(dcpe) naphthalene (**19**) where the nickel has a metal arene interaction with the ring of the naphthalene.

Scheme 3.7 Equilibrium reaction between 19 and Arenes

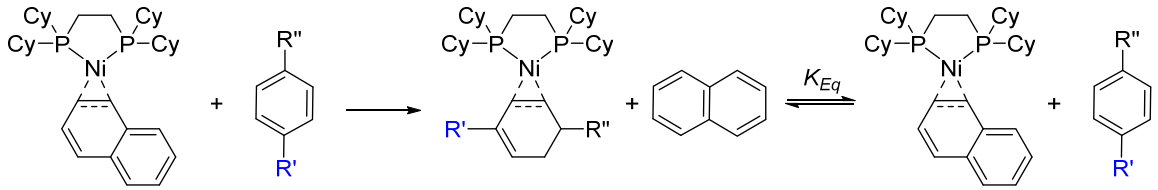

The goal was to measure the equilibrium constants of arene exchange in the nickel complex **19**. Treatment of **19** with large amounts of substituted arenes did indeed lead to arene exchange as observed by ^{31}P NMR spectroscopy (Table 3.7). The more electron withdrawing arenes were found to substitute more easily than less electron withdrawing arenes. Comparing 4-trifluoromethyltoluene and trifluoromethylbenzene one can see that the electron withdrawing groups shift the equilibrium in favor of the arene binding. 4-trifluoromethylanisole was found to bind to nickel more preferentially

than 4-trifluoromethyltoluene. This could be due to interaction with the anisole or due to the anisole moiety while being σ_p donating is actually σ_m withdrawing in comparison to the methyl group (σ_m 0.12 and -0.07 for OMe and Me groups respectively).[21] This would cause the meta position of the ring to be a site of low electron density allowing the nickel to interact with the ring. 1,4-ditrifluoromethylbenzene was found to be one of the few substrates tried that easily displaced naphthalene.

K_{eq}	$Arene_{CF}$
12.1	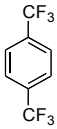
0.003	
0.0015	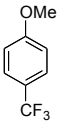
0.0008	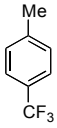

Table 3.7 Equilibrium constants for **19** with listed arenes

The equilibrium constants clearly show that the equilibrium is influenced greatly by the electron withdrawing groups. This provides support for our proposal that the substrate equilibrium plays a part in the rate acceleration observed in the catalytic systems.

CONCLUSIONS:

The kinetics of oxidative addition was studied using the previously studied nickel(0) terphenyl diphosphine model complexes. Formaldehyde was found to negatively affect the kinetics at certain temperatures. Kinetics were carried out in the presence of a Grignard reagent in order to prevent formaldehyde formation. The rates of oxidative addition were found to be similar amongst the three model systems. The trifluoromethyl was only three times slower than the tert-butyl and dimethylamino. Activation parameters were similar across the three complexes. The similarity of the kinetics and activation parameters was postulated to be due to stabilization of the ground state and oxidative addition transition state in the model complex. Unfortunately we were unable to determine the actual rates of oxidative addition in the catalytic systems, but using our model system in conjunction with the catalytic systems we were able to show that oxidative addition in the model system is unaffected by the electronics of the arene. While oxidative addition in the catalytic system shows a significant variance in rate depending on the electronics of the substrate arene, we were able to show that this is in part due to a shifting of the pre-equilibrium of the substrate.

EXPERIMENTAL SECTION:

General considerations: Unless otherwise specified, all compounds were manipulated using a glove box under a nitrogen atmosphere. Solvents for all reactions were dried by Grubbs' method. Benzene-d6 was purchased from Cambridge Isotope Laboratories and vacuum distilled from sodium benzophenone ketyl. All other materials were used as received. $Ni(II)Cl_2(PCy_3)_2$ was purchased from Strem Chemicals as a crystalline solid and was used as received. ^{1}H, ^{13}C, and ^{31}P NMR spectra were recorded on a Varian Mercury 300 spectrometer at ambient temperature, unless denoted otherwise. Chemical shifts are reported with respect to internal solvent: 7.16 ppm and 128.06 (t) ppm (C6D6) and for ^{1}H and ^{13}C NMR data, respectively. ^{31}P NMR chemical shifts are reported with respect to the instrument solvent lock when a deuterated solvent was used. IR spectra were recorded on a Thermo-Fisher Scientific Nicolet 6700 FT-IR spectrometer. Gas chromatography-mass spectrometry (GC-MS) analysis was performed upon filtering the sample through a plug of silica gel. Fast atom bombardment-mass spectrometry (FAB-MS) analysis was performed with a JEOL JMS-600H high-resolution mass spectrometer.

Synthesis of [1,3-bis(2'-diisopropylphosphino)-4-dimethylamino-2-methoxybenzene]nickel(0)carbonyl (16)

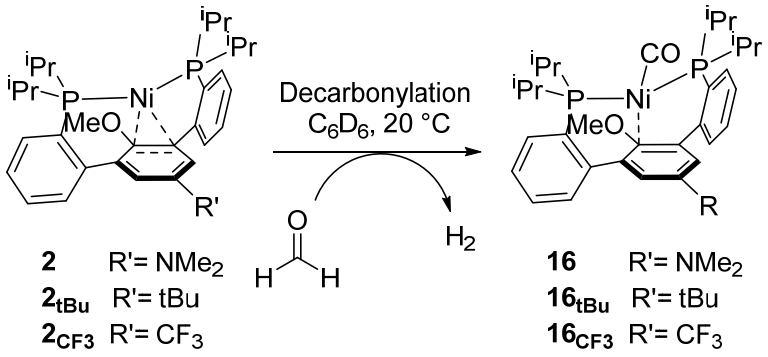

To a solution of **2** (12.3 mg, 0.021 mmol) in C_6D_6 was added 5 equivalents of formaldehyde (3.7 mg, 0.123 mmol). Upon addition hydrogen gas was vigorously evolved as the solution turned from dark red, to red orange in a matter of minutes. The solvent was removed *in vacuo* and the residue was washed with hexanes and eluted with ether. The solvent was removed from the orange ether fraction resulting in an orange residue of **16**.

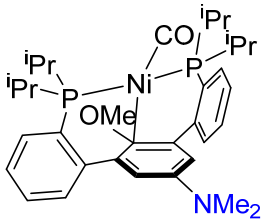

16 Yield: (11.3 mg, 0.018 mmol 87.1 %) ^{1}H NMR (C_6D_6, 300 MHz) δ 7.47 (br m, 4H, Ar-*H*), 7.22 (br m, 4H, Ar-*H*), 6.58 (br s, 2H, Ar-*H*) 2.67 (s, 6H, N(C*H*$_3$)$_2$), 2.57 (s, 3H, OC*H*$_3$), 2.48 (septet, 1H, C*H*(CH$_3$)$_2$), 2.15 (septet, 1H, C*H*(CH$_3$)$_2$), 1.25 (septet, 18H, C*H*(CH$_3$)$_2$), 0.99 (septet, 6H, C*H*(CH$_3$)$_2$), ^{13}C{^{1}H} NMR (C_6D_6, 100.54 MHz) δ 194.01 (t, Ni-*C*O), 149.57 (s, Ar-*C*$_4$), 147.94 (t, Ar-*C*$_{10}$), 138.45 (s, Ar-*C*$_2$), 136.27 (t, Ar-*C*$_5$), 130.33 (s, Ar-*C*$_9$), 129.90 (s, Ar-*C*$_6$), 127.95 (s, Ar-*C*$_8$), 126.97 (s, Ar-*C*$_7$), 122.79 (s,

Ar-*C*$_3$), 113.60 (s, Ar-*C*$_1$), 60.59 (s, Ar-*OMe*), 40.91 (N(*C*H$_3$)$_2$), 29.48 (*C*H-(CH$_3$)$_2$), 26.08 (*C*H-(CH$_3$)$_2$), 19.42 (CH-(*C*H$_3$)$_2$), 19.14 (CH-(*C*H$_3$)$_2$), 18.86 (CH-(*C*H$_3$)$_2$), 18.03 (CH-(*C*H$_3$)$_2$), ^{31}P{^{1}H} NMR δ 36.25 Anal. Calcd. for $C_{34}H_{47}NNiO_2P_2$ (%): C, 65.61; H, 7.61; N, 2.25 Found C, 68.73; H, 7.41; N, 2.09.

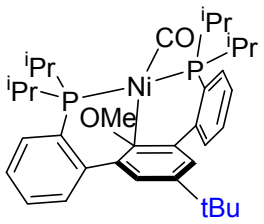

16$_{tBu}$. Yield: (10.2 mg, 0.016 mmol 85.0 %) ^{1}H NMR (C_6D_6, 300 MHz) δ 7.44 (br m, 4H, Ar-*H*), 7.21 (br m, 6H, Ar-*H*), 2.49 (s, 3H, OC*H*$_3$) 2.46 (s, 1H, C*H*(CH$_3$)$_2$), 2.15 (s, 1H, C*H*(CH$_3$)$_2$), 1.43 (s, 6H, N(CH$_3$)$_2$), 1.20 (m, 18H, CH(C*H*$_3$)$_2$), 0.95 (m, 6H, CH(C*H*$_3$)$_2$), ^{13}C{^{1}H} NMR (C_6D_6, 100.54 MHz) δ 194.80 (t, Ni-*C*O), 148.30 (s, Ar-*C*$_4$), 146.26 (t, Ar-*C*$_{10}$), 137.23 (s, Ar-*C*$_2$), 130.65 (t, Ar-*C*$_5$), 130.27 (s, Ar-*C*$_9$), 129.84 (s, Ar-*C*$_6$), 128.67 (s, Ar-*C*$_8$), 126.91 (s, Ar-*C*$_7$), 125.88 (s, Ar-*C*$_3$), 60.21 (s, Ar-*OMe*), 34.15 (*C*(CH$_3$)$_2$), 31.36 (C(*C*H$_3$)$_2$), 29.35 (*C*H-(CH$_3$)$_2$), 25.55 (*C*H-(CH$_3$)$_2$), 19.19 (CH-(*C*H$_3$)$_2$), 18.89 (CH-(*C*H$_3$)$_2$), 18.72 (CH-(*C*H$_3$)$_2$), 17.77 (CH-(*C*H$_3$)$_2$) ^{31}P{^{1}H} NMR δ 35.92

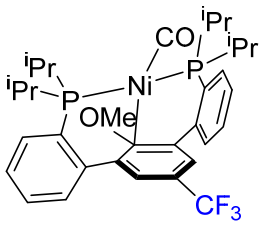

16$_{CF3}$. Yield: (13.4 mg, 0.021 mmol 92.7 %) ^{1}H NMR (C_6D_6, 300 MHz) δ 7.34 (br s, 2H, Ar-*H*), 7.32 (m, 2H, Ar-*H*), 7.23 (m, 2H, Ar-*H*), 7.15 (m, 2H, Ar-*H*), 2.42 (s, 3H, OC*H*$_3$) 2.39 (s, 2H, C*H*(CH$_3$)$_2$), 2.05 (s, 2H, C*H*(CH$_3$)$_2$), 1.11 (s, 12H, CH(C*H*$_3$)$_2$), 1.03 (m, 6H, CH(C*H*$_3$)$_2$), 0.82 (m, 6H, CH(C*H*$_3$)$_2$), ^{13}C{^{1}H} NMR (C_6D_6, 100.54 MHz) δ

195.52 (t, Ni-*C*O), 147.79 (s, Ar-*C*$_4$), 147.58 (t, Ar-*C*$_{10}$), 135.69 (s, Ar-*C*$_2$), 130.14 (t, Ar-*C*$_5$), 139.64 (s, Ar-*C*$_9$), 129.64 (s, Ar-*C*$_6$), 129.17 (s, Ar-*C*$_8$), 127.41 (s, Ar-*C*$_7$), 124.10 (s, Ar-*C*$_3$), 123.91 (Ar-*C*F$_3$), 120.26 (s, Ar-*C*$_1$), 59.96 (s, Ar-*OMe*), 28.78 (*C*H-(CH$_3$)$_2$), 24.78 (*C*H-(CH$_3$)$_2$), 18.82 (CH-(*C*H$_3$)$_2$), 18.52 (CH-(*C*H$_3$)$_2$), 18.42 (CH-(*C*H$_3$)$_2$), 17.44 (CH-(*C*H$_3$)$_2$), ^{19}F{^{1}H} NMR δ -61.30, ^{31}P{^{1}H} NMR δ 37.25 Anal. Calcd. for $C_{33}H_{11}F_3NiO_2P_2$ (%): C, 61.23; H, 6.38; Found C, 55.83; H, 6.12.

Synthesis of bis[bis(tricyclohexylphosphine)nickel] dinitrogen (18)

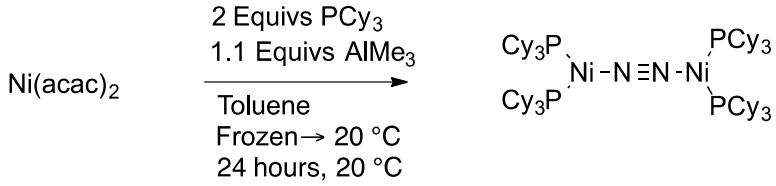

A modified literature procedure was used for the synthesis of **18**.[20] To a freshly thawed mixture of Ni(acac)$_2$ (1.00 g, 3.89 mmol) and tricyclohexylphosphine (2.19 g, 7.81 mmol) in 12 ml of toluene was added a thawed solution of AlMe$_3$ (315 mg, 4.38 mmol) in 3 ml of toluene. Upon addition of AlMe$_3$ the blue green solution turned dark red. The reaction vessel was stoppered and the reaction mixture was stirred for 24 hours. The after 24 hours the stirring was stopped and the reaction mixture was allowed to sit for 3 hours. The slurry was filtered through Celite and the solid was eluted with toluene. The flow through of the filtration was placed in the freezer to promote crystallization/precipitation. The toluene fraction was pumped down to give a dark red solid and was used as isolated. Yield: (814 mg, 1.28 mmol 33.2 %) ^{1}H NMR (C_6D_6, 300 MHz) δ 1.89 (br s, 12H, Cy-*H*), 1.72 (br m, 48H, Cy-*H*), 1.27 (br m, 72H, Cy-*H*) ^{31}P{^{1}H} NMR δ 45.98

Synthesis of 19

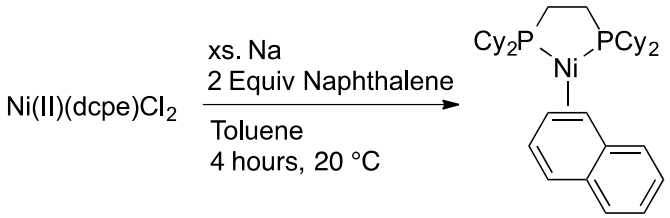

Naphthalene (47.5 mg, 0.37 mmol) was added to a vial containing a sodium mirror (65.3 mg 2.84 mmol) as a solution in THF. The sodium naphthalene solution immediately turned dark forest green. The sodium naphthalene was stirred for 30 minutes. In a separate vial Ni(II)(dcpe)Cl_2 (100.2 mg, 0.18 mmol) was stirred as a slurry in THF. The dark green sodium naphthalene solution was added to the Ni(II)(dcpe)Cl_2 mixture. The solution slurry turned from dark green to yellow and finally to red orange. The mixture was stirred for 45 minutes before filtering through Celite. The solvent was removed resulting in a red orange solid. The residue was washed with pentane and eluted with benzene resulting in 18. Yield: (203.8 mg, 88.2%) ^{1}H NMR (C_6D_6, 300 MHz) δ 7.37 (br s, 2H, Ar-*H*), 7.08 (br s, 2H, Ar-*H*), 5.85 (br d, 4H, Ar-*H*), 1.62 (br d, 32H, (dcpe)-*H*), 1.12 (br s, 20H, (dcpe-*H*), ^{31}P{^{1}H} NMR δ 53.38 (dd, J = 717.9, 81.9 Hz)

Kinetic Studies:

Special considerations: All kinetic data over 45 °C was collected on a Varian INOVA-500 MHz NMR spectrometer and all 45°C kinetic data was collected using a Varian Mercury 300 MHz NMR spectrometer. In all experiments trimethoxybenzene was used as a standard.

Example of a Kinetic Reaction:

In a glove box a J-Young tube was charged with 11.3 mg (0.019 mmol) of **2** and 1.1 mg (0.006 mmol) of trimethoxybenzene in C_6D_6 or d_8-toluene. The J-Young tube was heated to the desired temperature in either an oil bath or in an NMR spectrometer. NMR spectra were collected at regular intervals.

Catalytic Studies:

Special Considerations: All catalytic reactions were performed using 1,3,5-tritert-butylbenzene as an internal standard. All conversions listed were calculated via amounts of analytes based on gas chromatography.

Example of a Catalytic Reaction:

In a glove box a Schlenk tube containing 40.2 mg (0.244 mmol) of tert-butyl anisole , 16.4 mg (0.024 mmol) $Ni(PCy_3)_2Cl_2$, 12.7 mg (0.045 mmol) of PCy_3, and 61.2 mg (0.025 mmol) of 1,3,5-tritert-butylbenzene was charged with 2.7 ml of dry toluene. This solution was allowed to stir for five minutes before 300 µl of MeMgBr (3M in Et_2O) was added via syringe. The slurry immediately turned yellow. The Schlenk was sealed and heated to 80°C for 17 hours after which the reaction was quenched with water and the organics were extracted by DCM. The organic fraction was analyzed via gas chromatography.

Example of an Equilibrium Reaction:

In a glove box a J-Young tube containing 10.3 mg of **19** (0.017 mmol) was treated with 10 equivalents of naphthalene and one equivalent of 1,4-ditrifluorobenzene in C_6D_6. The solution was mixed by shaking. The mixture was analyzed by ^{31}P NMR spectroscopy and the concentration of the resulting species was calculated. Using the observed concentrations of the nickel species and the added concentrations of the naphthalene and substituted benzene the equilibrium constants were calculated.

REFERENCES

1. Rosen, B. M.; Quasdorf, K. W.; Wilson, D. A.; Zhang, N.; Resmerita, A.-M.; Garg, N. K.; Percec, V. *Chemical Reviews* **2010**, *111*, 1346-1416.
2. Álvarez-Bercedo, P.; Martin, R. *Journal of the American Chemical Society* **2010**, *132*, 17352-17353.
3. Guan, B.-T.; Wang, Y.; Li, B.-J.; Yu, D.-G.; Shi, Z.-J. *Journal of the American Chemical Society* **2008**, *130*, 14468-14470.
4. Guan, B.-T.; Xiang, S.-K.; Wu, T.; Sun, Z.-P.; Wang, B.-Q.; Zhao, K.-Q.; Shi, Z.-J. *Chemical Communications* **2008**, 1437-1439.
5. Hie, L.; Ramgren, S. D.; Mesganaw, T.; Garg, N. K. *Organic Letters* **2012**, *14*, 4182-4185.
6. Quasdorf, K. W.; Antoft-Finch, A.; Liu, P.; Silberstein, A. L.; Komaromi, A.; Blackburn, T.; Ramgren, S. D.; Houk, K. N.; Snieckus, V.; Garg, N. K. *Journal of the American Chemical Society* **2011**, *133*, 6352-6363.
7. Quasdorf, K. W.; Tian, X.; Garg, N. K. *Journal of the American Chemical Society* **2008**, *130*, 14422-14423.
8. Tobisu, M.; Yamakawa, K.; Shimasaki, T.; Chatani, N. *Chemical Communications* **2011**, *47*, 2946-2948.
9. Dankwardt, J. W. *Angewandte Chemie International Edition* **2004**, *43*, 2428-2432.
10. Tamao, K.; Sumitani, K.; Kiso, Y.; Zembayashi, M.; Fujioka, A.; Kodama, S.-i.; Nakajima, I.; Minato, A.; Kumada, M. *Bulletin of the Chemical Society of Japan* **1976**, *49*, 1958-1969.
11. Tamao, K.; Sumitani, K.; Kumada, M. *Journal of the American Chemical Society* **1972**, *94*, 4374-4376.
12. Hartwig, J. F. *Inorganic Chemistry* **2007**, *46*, 1936-1947.
13. Culkin, D. A.; Hartwig, J. F. *Organometallics* **2004**, *23*, 3398-3416.
14. Sergeev, A. G.; Hartwig, J. F. *Science* **2011**, *332*, 439-443.
15. Kelley, P.; Lin, S.; Edouard, G.; Day, M. W.; Agapie, T. *Journal of the American Chemical Society* **2012**, *134*, 5480-5483.
16. Littke, A. F.; Fu, G. C. *Angewandte Chemie International Edition* **2002**, *41*, 4176-4211.
17. Stambuli, J. P.; Kuwano, R.; Hartwig, J. F. *Angewandte Chemie International Edition* **2002**, *41*, 4746-4748.
18. Saito, S.; Oh-tani, S.; Miyaura, N. *The Journal of Organic Chemistry* **1997**, *62*, 8024-8030.
19. Amatore, C.; Pfluger, F. *Organometallics* **1990**, *9*, 2276-2282.
20. Jolly, P. W.; Jonas, K.; Krüger, C.; Tsay, Y. H. *Journal of Organometallic Chemistry* **1971**, *33*, 109-122.
21. Corwin, H.; Leo, A.; Taft, R. W.; *Chemical Review* **1991**, *91*, 165-195.